Eur. Phys. J. D **22**, 199–207 (2003)
DOI: 10.1140/epjd/e2003-00013-1

THE EUROPEAN PHYSICAL JOURNAL D

Experimental determination of spin-rotation and spin-spin magnetic interactions in $^{13}CH_3F$ by nuclear spin conversion

P. Cacciani[a], J. Cosléou, F. Herlemont, M. Khelkhal, and J. Legrand

Laboratoire de Physique des Lasers, Atomes et Molécules, CERLA, Centre Lasers et Applications, Université des Sciences et Technologies de Lille, 59655 Villeneuve d'Ascq Cedex, France

Received 23 May 2002 / Received in final form 18 September 2002
Published online 21 January 2003 –

Abstract. When a gas sample of $^{13}CH_3F$ is prepared with a population of isomers (ortho and para forms) far from the equilibrium given by nuclear spin statistics, it relaxes towards this equilibrium with an exponential decay rate. This phenomenon called nuclear spin conversion is mainly governed by intramolecular spin-spin and spin-rotation interactions. In the quantum relaxation model [P.L. Chapovsky, Phys. Rev. A **43**, 3624 (1991)], two pairs of ortho-para levels ($J = 9$, $K = 3$; $J' = 11$, $K' = 1$) and ($J = 20$, $K = 3$; $J' = 21$, $K' = 1$) are principally responsible for the conversion. The levels of the second pair are coupled by both spin-spin and spin-rotation interactions. The application of an electric field (up to 10 kV/cm) induces a crossing of the Stark components of this pair, which is observed for the first time. A specific experimental set-up based on an electric field of alternating triangular shape is used, which allows the determination of the strength of both interactions *via* the measurement of the spin conversion decay rates. This work yields the first experimental value for the electronic contribution to the spin-rotation interaction in $^{13}CH_3F$.

PACS. 31.30.Gs Hyperfine interactions and isotope effects, Jahn-Teller effect – 33.80.Be Level crossing and optical pumping – 34.30.+h Intramolecular energy transfer; intramolecular dynamics; dynamics of van der Waals molecules

1 Introduction

The existence of nuclear spin isomers for molecules having several equivalent atoms with non zero nuclear spin is the consequence of Pauli's principle and is responsible for the intensity alternation of spectral lines well known in spectroscopy. The corresponding nuclear spin states are very stable in the gas phase. A change of the total nuclear spin requires the presence of a strong magnetic field gradient on the molecular scale. Such gradients can occur within a molecule *via* spin-spin and spin-rotation magnetic interactions or through intermolecular potentials due to a paramagnetic partner. Thus, studying nuclear spin conversion could be an efficient way to derive information relating to these interactions.

Such studies are very rare and available for very few molecules. The main requirement for observing spin conversion is the capability to separate the isomers or at least to enrich a gas sample in one specific species. This has been observed with different techniques only for H_2 [1] (cooling in the presence of a magnetic catalyst), CH_3F [2] and C_2H_4 [3] (light induced drift LID), CH_2O [4] (selective photolysis), H_2O [5], H_3^+ [6] and Li_2 [7] (chemical reaction from enriched reactant).

The most frequently studied molecule has been CH_3F, which has C_{3v} symmetry and consequently two spin configurations, ortho (total nuclear spin $I = 3/2$) and para ($I = 1/2$). Interest in this molecule arises from its well defined spectroscopy and the coincidence of some absorption lines with CO_2 laser transitions, which allows significant enrichment (5% to 10%) with the LID technique [8].

Different experimental observations have helped to explain the mechanism behind spin conversion. For CH_3F, the conversion rate is found to be proportional to the gas pressure (12×10^{-3} s^{-1}/torr for $^{13}CH_3F$ and 3×10^{-4} s^{-1}/torr for $^{12}CH_3F$ at 300 K). This conversion rate is slightly reduced if part of the gas is substituted by paramagnetic O_2 whereas it stays constant if the substitution is made by molecules with a large dipole moment such as CH_3Cl [8]. This indicates that intermolecular processes are not directly involved in spin-conversion of CH_3F although collisions play a role in the mechanism.

Intramolecular wavefunction mixing induced by spin-rotation or spin-spin interactions was first considered by Curl *et al.* [9] as an important pathway for the equilibration of nuclear spin statistics isomers. Following this idea, Chapovsky [10] proposed a mechanism called "quantum

[a] e-mail: Patrice.Cacciani@univ-lille1.fr

relaxation" which combines the usual relaxation by collisions with internal quantum properties of the molecule. Let us recall its essence for the convenience of the reader. Intramolecular magnetic perturbations (spin-spin and spin-rotation) couple some pairs of quasi-degenerate ortho and para states. Due to this coupling, some eigenstates are no longer purely ortho or para but mixed states. Suppose that at the instant $t = 0$ a test molecule is in the ortho subspace. Due to collisions with other particles, the test molecule starts a migration among rotational states but only within the ortho subspace, as a collision is unable to produce direct transition from the ortho to the para subspace. This is the common phenomenon of rotational relaxation. Exploring the ladder of all ortho states, the test molecule can reach by collision an ortho level α coupled by intramolecular interaction with the energetically close para level α'. During free flight following this collision, an evolution of the wavefunction takes place with mixed states as eigenstates, and the wavefunction describing the test molecule is the ortho state α with a small admixture of the para state α'. The next collision stops this evolution and a probability linked to this admixture exists to transfer the molecule into a pure para state, which thus localizes it inside the para subspace.

A quantitative description of the conversion process has been developed in the framework of the density matrix formalism [10]. The relaxation of a non-equilibrium concentration of, *e.g.* ortho molecules, $\delta\rho_0(0)$ created at the instant $t = 0$ will decay exponentially:

$$\delta\rho_0(t) = \delta\rho_0(0)\mathrm{e}^{-\gamma t} \tag{1}$$

where γ is the conversion rate expressed as

$$\gamma = \sum_{\alpha\in\text{ortho},\,\alpha'\in\text{para}} \frac{2\Gamma_{\alpha\alpha'}|V_{\alpha\alpha'}|^2}{\Gamma_{\alpha\alpha'}^2+\omega_{\alpha\alpha'}^2}\left[W_\mathrm{B}(\alpha)+W_\mathrm{B}(\alpha')\right]. \tag{2}$$

The summation has to be made over all ortho and para level pairs (α, α'), $V_{\alpha\alpha'}$ is the matrix element of the interaction expressed in $\hbar$ units, W_B is the Boltzmann factor, $\hbar\omega_{\alpha\alpha'}$ is the energy difference between the levels of the pair and $\Gamma_{\alpha\alpha'}$ is the collisional decay rate of the off-diagonal element of the density matrix $\rho_{\alpha\alpha'}$. The validity of this first order model holds with the condition $|V_{\alpha\alpha'}| \ll \max\left(|\omega_{\alpha\alpha'}|, \Gamma_{\alpha\alpha'}\right)$ [11] which is the case even in our low pressure experimental conditions.

$^{13}CH_3F$ presents two pairs of ortho-para levels which can be coupled by spin-spin and/or spin-rotation interactions. Several experimental confirmations of this model have been performed, such as the influence of the temperature or an increased conversion rate in the presence of an electric field [8,12,13]. Although the collisional decay rate $\Gamma_{\alpha\alpha'}$ is still a parameter difficult to evaluate or measure, the confidence in the mechanism now allows us to use the conversion process as a tool to measure fundamental intramolecular interactions.

As reported in a previous contribution [14], we have developed an experimental technique using a triangular alternating field leading to the determination of the strength of the interactions without relying on a knowledge of $\Gamma_{\alpha\alpha'}$. The set-up was such that only a moderate electric field could be applied. For this reason only crossings of Stark sublevels of the closest ortho-para pair of $^{13}CH_3F$ were reached, leading to the determination only of the spin-spin interaction. Some experimental improvements have recently been achieved to reach crossings for the second pair which involves both spin-spin and spin-rotation interactions.

The aim of this paper is to present how both magnetic interaction strengths can be deduced from conversion rate measurements. It is organized as followed: in the next section, the nature of the two magnetic interactions is recalled, then the behaviour of the conversion rate in the presence of an electric field is calculated in the two cases of a static and a triangular alternating field used in the experiment. The experiment is described in Section 4 with the specific aspects of the new design. Experimental results are given in Section 5 and compared to the calculation. Finally spin-spin and spin-rotation interaction strengths are derived and their uncertainties issuing from the experimental procedure are discussed.

2 Spin-spin and spin-rotation magnetic interactions

These interactions are of fundamental interest. The first one can be calculated through the mutual interactions of the nuclear magnetic dipoles $\widehat{\mu} = \mu\widehat{\mathbf{S}}/S$. The coupling term is usually written as:

$$\begin{aligned} V_{1,2} &= \frac{\mu_0}{4\pi}\frac{1}{r_{12}^3}\left[\widehat{\mu_1}\cdot\widehat{\mu_2} - 3\left(\widehat{\mu_1}\cdot\widehat{\mathbf{n}}\right)\left(\widehat{\mu_2}\cdot\widehat{\mathbf{n}}\right)\right] \\ &= P_{12}\left[\widehat{\mathbf{S}}_1\cdot\widehat{\mathbf{S}}_2 - 3\left(\widehat{\mathbf{S}}_1\cdot\widehat{\mathbf{n}}\right)\left(\widehat{\mathbf{S}}_2\cdot\widehat{\mathbf{n}}\right)\right] \\ &\text{with } P_{1,2} = \frac{\mu_0}{4\pi}\frac{\mu_1\mu_2}{S^{(1)}S^{(2)}}\frac{1}{r_{12}^3} \end{aligned} \tag{3}$$

where r_{12} is the distance between the particles, $S^{(i)}$ their nuclear spin and $\widehat{\mathbf{n}}$ the unit vector directed from the first particle to the second.

As we are focusing on ortho-para conversion linked to the total spin of hydrogen atoms, only interaction between one hydrogen atom and another atom (C, H, F) is kept and we leave out the possible C-F spin-spin interaction. ^{13}C has a non zero nuclear spin and the interaction between carbon and hydrogen has therefore to be considered in this work.

The spin-spin interaction depends on distances between nuclei through scaling factors P_{HH}, P_{CH}, P_{FH} and on tensorial properties of the vectorial part of the equation (3). Complete derivation of the interaction is shown in [10] and we just recall the notations in the following equations. $\widehat{\mathbf{S}}^{(m)}$, $\widehat{\mathbf{I}}$, $\widehat{\mathbf{R}}$ are respectively the spin operators of the mth hydrogen ($m = 1, 2, 3$), fluorine and carbon nuclei. The spatial tensors for interactions H_m–H_n, F–H_m, C–H_m are noted $T_{ij}^{(m,n)}$, $Q_{ij}^{(m)}$, $\theta_{ij}^{(m)}$ respectively. Thus,

Table 1. Parameters of the two pairs involved in nuclear spin conversion in $^{13}CH_3F$.

J', K'/J, K	$\Delta J/\Delta K$	$\omega_{J'K'/JK}$(GHz)$^{(1)}$	$W_B{}^{(2)}$	Interaction
11, 1/9, 3	2/–2	0.13001	7.67×10^{-5}	$\mathcal{T}_{22}$
21, 1/20, 3	1/–2	0.35200	2.02×10^{-5}	$\mathcal{T}_{22}$, C_{22}

$^{(1)}$Reference [19], $^{(2)}$reference [24].

the spin-spin operators in the laboratory frame can be written:

$$\begin{aligned}\widehat{V}_{\mathrm{HH}} &= \sum_{m<n}\sum_{i,j}\widehat{S}_i^{(m)}\widehat{S}_j^{(n)}T_{ij}^{(m,n)} \quad m,n=1,2,3\\ \widehat{V}_{\mathrm{FH}} &= \sum_{m}\sum_{i,j}\widehat{S}_i^{(m)}\widehat{I}_j Q_{ij}^{(m)}\\ \widehat{V}_{\mathrm{CH}} &= \sum_{m}\sum_{i,j}\widehat{S}_i^{(m)}\widehat{R}_j\theta_{ij}^{(m)}.\end{aligned} \tag{4}$$

The second interaction, called spin-rotation, arises from the coupling of each nuclear spin with the magnetic field induced by the rotation of the charges within the molecule. Rotation of the nuclei gives a first contribution, and a less direct one is the contribution of the electron motion combining the molecular frame rotation with the fast motion relative to the molecule-fixed coordinate system.

Flygare [15] derived a formulation of the spin-rotation interaction in terms of a second rank tensor $\mathbf{C}$ coupled with the rotational and nuclear spin momenta:

$$H_{\mathrm{spin-rotation}} = \sum_n {}^n\mathbf{I}\cdot{}^n\mathbf{C}\cdot\mathbf{J} \tag{5}$$

where the sum runs over the n nuclei of the molecule. He mentioned the ability to express the tensor as the sum of a term depending on the equilibrium nuclear positions and a term depending on all the excited electronic states in the molecule. He also pointed out the relation between the spin-rotation tensor and the nuclear magnetic shielding tensor. More recent contributions [16,17] have rewritten the spin-rotation interaction in a symmetrized form and have decomposed ${}^n\mathbf{C}$ into two parts arising from the nuclear motion and the electronic motion, respectively:

$${}^n\mathbf{C} = {}^n\mathbf{N} + {}^n\mathbf{E}. \tag{6}$$

${}^n\mathbf{N}$ is obtained through a first order perturbation averaged over the vibronic ground state. It can be calculated precisely since the average nuclear positions and rotational parameters are well-known [18–20]. ${}^n\mathbf{E}$ arises in a second order perturbation treatment of the couplings of the electronic angular momenta with the nuclear spins and the rotational momentum. It involves the spectrum of all molecular rovibronic excited states (different from the ground state). As is noted in reference [16]: "it is almost impossible to calculate this tensor which will be considered as a set of electronic parameters to be measured experimentally. Their values are important, since they serve as useful tests of various electronic calculations performed within truncated basis sets".

In rotational or rovibrational spectroscopy, the nuclear quadrupole hyperfine structure, when it is present, is often well resolved. Conversely weaker effects such as spin-spin and spin-rotation interactions are usually not observed because they are beyond the limit of resolution of most spectrometers. Even when resolution allows such observation, only diagonal elements of the total spin-rotation tensor ${}^n\mathbf{C}$ can be measured by fitting the hyperfine spectrum [21]. The available information concerns the parallel ${}^nC_{zz}$ and perpendicular ${}^nC_\perp = ({}^nC_{xx} + {}^nC_{yy})/2$ diagonal components of the tensor of the hydrogen nuclei. However the off-diagonal ones ${}^nC_{xz}$, ${}^nC_{zx}$ and the transverse anisotropy defined by

$$\Delta^n C_\perp = \frac{{}^nC_{xx} - {}^nC_{yy}}{2}$$

cannot be reached in such experiments and remain unknown. Nuclear spin conversion gives an opportunity to measure such terms and it is the main motivation of our study.

For $^{13}CH_3F$, there are two main interacting pairs whose properties are described in Table 1. Let us recall that the symmetry of the wavefunction for C_{3v} symmetric top in its electronic and vibrational ground state is characterized by the K quantum number, where K is the projection of the angular momentum J on the molecular axis: $K = 3n$ (n integer) for ortho states, $K \neq 3n$ for para states. The first pair ($J = 9$ $K = 3$, $J' = 11$ $K' = 1$) only interacts by a spin-spin coupling which is characterized by the selection rule $\Delta J \leq 2$. The second pair ($J = 20$ $K = 3$, $J' = 21$ $K' = 1$) is coupled by both spin-spin and spin-rotation interactions for which the selection rule is $\Delta J \leq 1$ [16]. Furthermore, because $\Delta K = 2$ for this pair and for symmetry reasons, only the electronic part of the spin-rotation interaction, through the term $\Delta^n C_\perp = \Delta^n E_\perp$, is involved in the spin conversion process [16]. The difficulty of theoretical evaluation of such a term emphasizes the interest of its experimental determination.

3 Calculation of the conversion rate in an electric field

In the determination of the interaction terms from measurements of conversion rate, the main difficulty comes from the lack of information on the collisional decay rate $\Gamma_{\alpha,\alpha'}$ of the off-diagonal element of the density matrix. The assumption $\Gamma_{\alpha\alpha'} = (\Gamma_\alpha + \Gamma_{\alpha'})/2$ is usually made concerning the relaxation of the coherence created by

the magnetic interaction between ortho and para levels where Γ_α and $\Gamma_{\alpha'}$ are the relaxation rates of the population density of each separated spin isomer. All of these rates depend on the collision rate and vary linearly with the pressure. The determination of $\Gamma_{\alpha\alpha'}$ is still a problem which we have overcome by using an experimental technique [14] based on the following observation: in the summation (2), the Lorentzian form is such that if an integration over $\omega_{\alpha\alpha'}$ could be realized, the result will become independent of $\Gamma_{\alpha\alpha'}$. One can mimic this integration by applying an electric field with a triangular waveform. The energy difference of the level pairs changes linearly, $\hbar\omega_{\alpha\alpha'}(t) = \hbar\omega_0 + R_{\alpha\alpha'}Ff(t)$ where $R_{\alpha\alpha'}$ is the difference of the two slopes for ortho and para level energy *versus* the field. F is the amplitude of the field modulation, $Ff(t)$ is the field at time t where $f(t)$ is the triangular alternating function of period T with unit amplitude. $\hbar\omega_0$ is the energy difference at zero field.

One can show that, if the frequency of the alternating field is much larger than the spin conversion rate, the conversion is still described by an exponential decay with a rate $\gamma_{\rm St}$ averaged over each field experienced by the system. So the the integration in time yields the expected integration over ω:

$$\gamma_{\rm St} = \frac{1}{T}\int_0^T \frac{2\Gamma|V|^2}{\Gamma^2+\omega^2(t)}\,(W_{\rm B}+W'_{\rm B})\;{\rm d}t. \qquad (7)$$

The calculation has to take into account all the ortho-para pairs, and within one pair, all the possible M, M' sub-levels in interaction split by the electric field F. For CH_3F, which has a permanent electric dipole, each rotational state (J, K) has $2J+1$ components with first order energy shifts given by

$$E(J,K,M) = -F\mu\frac{MK}{J(J+1)}, \qquad (8)$$

where μ is the electric dipole moment, equal to 1.8579 Debye or 6.193×10^{-30} Cm. The energy gap at time t between the ortho J, K, M and para J', K', M' sublevels is then expressed as:

$$\hbar\omega_{\alpha M,\,\alpha' M'}(t) = \hbar\omega_{\alpha\alpha'} - F\,f(t)\mu\left(\frac{MK}{J(J+1)} - \frac{M'K'}{J'(J'+1)}\right) \qquad (9)$$

where $\hbar\omega_{\alpha\alpha'}$ is the energy gap at zero field. In this notation, α indicates the $(J,\,K)$ ortho state, α' indicates the $(J',\,K')$ para state and the subscript M or M' is added when the parameter depends on the sub-levels. The conversion rate is then expressed as:

$$\gamma_{\rm St} = \sum_{(\alpha,M),\,(\alpha',M')} \frac{1}{T}\int_0^T \frac{2\Gamma_{\alpha\alpha'}|V_{\alpha M,\,\alpha' M'}|^2}{\Gamma^2_{\alpha\alpha'}+\left(\omega_{\alpha M,\,\alpha' M'}(t)\right)^2} \times (W_\alpha + W_{\alpha'})\;{\rm d}t. \qquad (10)$$

This formula calls for some comments: the Boltzmann factor in principle depends on the M sub-level, but considering that the Stark energy is much lower than the kinetic energy kT, $W_{\alpha M}$ will be considered as independent of M; $\Gamma_{\alpha\alpha'}$ is taken independent of M, M'; this is strictly valid in the absence of field as a consequence of the spherical symmetry of the medium, but this assumption should be revised in the presence of an electric [22] or magnetic field. $V_{\alpha M,\,\alpha' M'}$ is the matrix element of the spin-spin and spin-rotation interaction and can be written [23,24]:

$$\begin{aligned}|V_{\alpha M,\alpha' M'}|^2 &= |V^{\rm spin-spin}_{\alpha M,\alpha' M'}|^2 + |V^{\rm spin-rotation}_{\alpha M,\alpha' M'}|^2 \\ &= \sum_{q=1,\,2}(2J+1)(2J'+1) \\ &\quad\times \begin{pmatrix} J' & J & 2 \\ -K' & K & q\end{pmatrix}^2 \begin{pmatrix} J' & J & 2 \\ -M' & M & \Delta M\end{pmatrix}^2 \mathcal{T}^2_{2q} \\ &\quad + \sum_{q=1,\,2}(2J+1)(2J'+1)(J+J'+3)(J+J'-1) \\ &\quad\times \begin{pmatrix} J' & J & 1 \\ -M' & M & \Delta M\end{pmatrix}^2 \begin{pmatrix} J' & J & 2 \\ -K' & K & q\end{pmatrix}^2 C^2_{2q}. \qquad (11)\end{aligned}$$

(:::) stands for the $3j$-symbol; $q = \Delta K = K' - K$ and depends on the pair considered. Selections rules are $|\Delta K|$, $|\Delta J|$, $|\Delta M| \le 2$ for spin-spin interaction and $|\Delta K| \le 2$, $|\Delta J|$, $|\Delta M| \le 1$ for spin-rotation. For $^{13}CH_3F$, involving two pairs with $|\Delta K| = 2$, the interaction term only involves two parameters, the spherical component of the spin-spin interaction second rank tensor $\mathcal{T}_{22}$ and the spherical component of the spin rotation tensor C_{22}.

To illustrate the advantage of the technique of triangular alternating field, we compare in Figure 1 the results of two simulated spectra for two different pressures, 0.1 and 0.3 torr; in the upper part, the usual conversion spectrum which represents the conversion rate γ_F in the presence of a static field F *versus* the strength of the field and in the lower part the result of the integration by the alternating triangular field of amplitude F as given by equation (10).

For these calculations, we have used the theoretical value of $\mathcal{T}_{22} = 69.2$ kHz calculated from the structure averaged in the vibrational ground state [18,20] and from each spin-spin contribution (H–H, C–H and F–H) (Eq. (4)). It is expressed as:

$$\mathcal{T}^2_{22} = 3\left|P_{\rm HH}T^{(1,2)}_{22}\right|^2 + 2\left|P_{\rm HF}Q^{(1)}_{22}\right|^2 + 2\left|P_{\rm HC}\theta^{(1)}_{22}\right|^2 \qquad (12)$$

where superscripts stand for the hydrogen nuclei. The scale factors are $P_{\rm HH} = 20.46$ kHz, $P_{\rm FH} = 13.68$ kHz and $P_{\rm CH} = 22.75$ kHz, whereas the spherical tensors are $T^{(1,2)}_{22} = -3/2{\rm e}^{-2\pi/3}$, $Q^{(1)}_{22} = 0.4$ and $\theta^{(1)}_{22} = 1.346$.

As no such information is available for the spin-rotation transverse anisotropy $C_{22} = \Delta^n C_\perp = \Delta^n E_\perp$, we use the value 2.1 kHz for C_{22} estimated from comparison between calculation and experiment [17]. For the relaxation rate of the coherence $\Gamma_{\alpha\alpha'}$ we use the values of reference [25] taking into account a J dependence, $\Gamma_{\alpha\alpha'}/P = 1.09\times10^8$ s^{-1}/torr for the first pair and $\Gamma_{\alpha\alpha'}/P = 1.00\times10^8$ s^{-1}/torr for the second one.

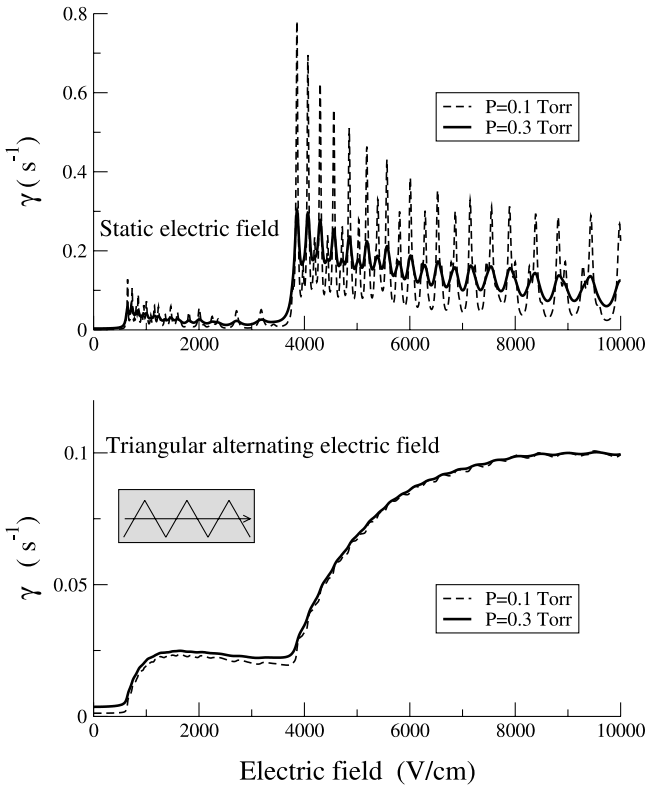

Fig. 1. Comparison between conversion spectra of $^{13}CH_3F$ calculated with a static electric field (upper part) and an alternating triangular electric field (lower part).

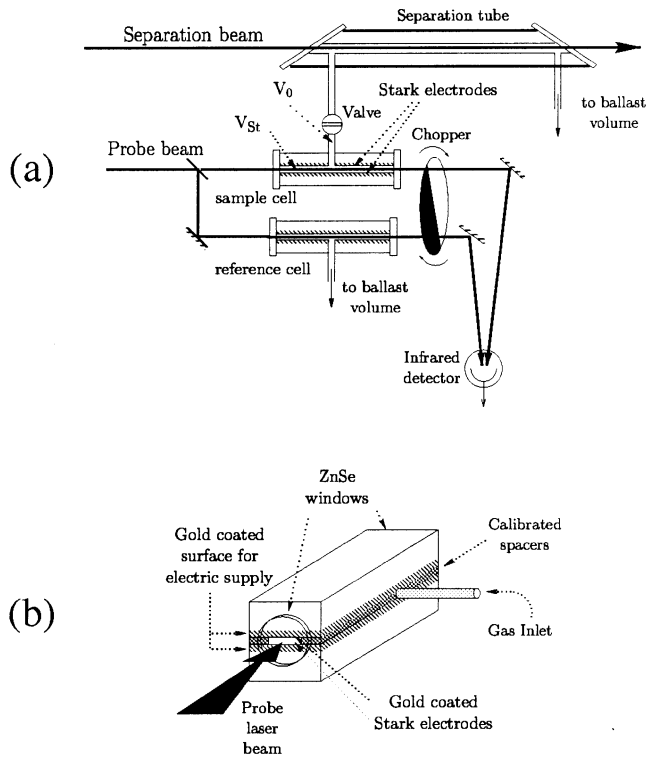

Fig. 2. Experimental set-up and detailed description of the Stark cell.

Both of these calculated spectra show clearly the presence of the two pairs with a sharp increase of the conversion rate around 600 V/cm and 4 000 V/cm. The influence of the pressure through $\Gamma_{\alpha\alpha'}$ behaves differently. The conversion spectrum in the upper part of the figure is made of peaks, each representing an individual crossing of M, M' sub-levels. The spectrum is smoothed for higher pressure as the width of each peak increases with pressure while its height consequently decreases keeping the area constant. In the lower part of the figure where a triangular field is applied, the conversion rates are lower, but the pressure dependence is almost removed except around zero field.

So, experimental data points obtained with a static field would be very sensitive to the exact value of the relaxation rate $\Gamma_{\alpha\alpha'}$. On the other hand, Stark integration removes the influence of this term and the knowledge of the two plateaus can then give direct information about both the spin-spin $\mathcal{T}_{22}$ and the spin rotation C_{22} interaction strengths.

4 Experimental set-up

The experimental set-up is schematically described in Figure 2a. The first stage of the experiment is the enrichment of the sample (isotopic purity 99%) by light induced drift (LID). This is performed by a powerful CO_2 laser (Edinburgh Instruments model PL5) tuned to the 9P(32) line with a typical power of 20 W. The center of this emission line is located on the edge of the absorption line R(4,3) (ortho isomer) of the ν_3 fundamental band of the $^{13}CH_3F$ molecule. The laser light enters the separation tube (glass tube with an inner diameter of 1 mm and 1 m long). The ortho isomer enrichment is transferred to the sample cell connected to one end of the separation tube. The ortho population disequilibrium in the sample is measured by comparing the absorption of a laser beam resonant with a line of the ortho isomer with its absorption in a reference cell. This cell is geometrically identical to the sample cell (10 cm long, 1 cm width, 0.08 cm between the electrodes) but connected to a ballast volume of the gas where the population of the two isomers always remains in equilibrium. A chopper (220 Hz) is used to send towards the same detector the beams going alternatively through the sample cell and the reference cell. The differential signal is detected by a lock-in amplifier. The enrichment by LID is observed through a disequilibrium of the two absorbed beams (phase I in Fig. 3). The second stage of the experiment is to isolate the enriched sample by closing the valve between the separation tube and the sample cell. The signal follows the evolution of the isomer composition of the sample, the enrichment decreases exponentially with a characteristic time inversely proportional to the conversion rate (phase II in Fig. 3).

In the previous set-up [14] a Stark cell was simply connected to the sample cell to study the conversion with an electric field, taking into account the volumes with and without field. This experimental configuration is valid as

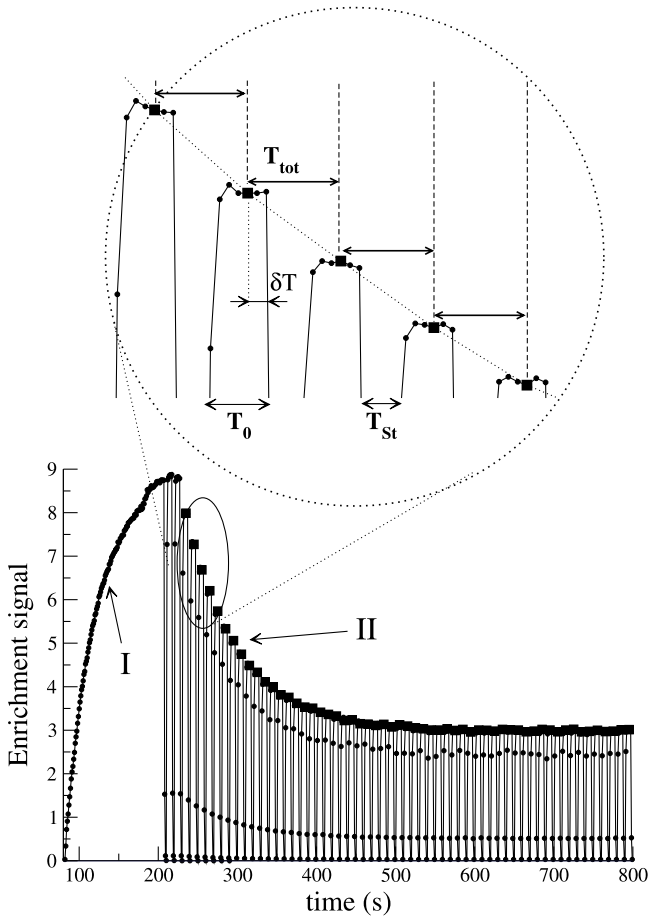

Fig. 3. Phase I: enrichment by LID; phase II: spin conversion in the presence of electric field with typical temporal scheme: dots are the data points taken every second, $T_0 = 7$ s is the duration without field, $T_{\rm St} = 3$ s is the duration when the alternating electric field is applied (the lock-in amplifier is off). The square data points are chosen separated by $T_{\rm tot} = T_{\rm St} + T_0$ and used for the fit of the rate $\gamma_{\rm exp}$.

long as the diffusion time from the sample cell to the Stark cell is small compared to the conversion rate in the electric field. This condition was found to fail for electric field greater than 1 200 V/cm.

To perform measurements at higher field strength, we have designed another set-up where the electric field is applied within the sample and reference cells to avoid problems due to the diffusion time. The frequency of the alternating triangular field was 100 Hz. This value, much larger than the conversion rates in the presence of the electric field, fulfilled the condition of validity of equation (7). Reducing the spacing between electrodes allows the application of field amplitude up to 10 kV/cm (see Fig. 2b). Unfortunately, such a configuration has its drawbacks. The detection technique is efficient if the probe laser frequency is resonant with one spin isomer only. In the presence of the electric field, the resonant transition is split into its Stark components, and keeping the same probe laser wavelength (efficient at zero field) the difference in absorption of the two species decreases and the overall sensitivity of the set-up is strongly reduced.

For this reason we have used a specific temporal sequence: the field is applied during a duration $T_{\rm St}$ where no measurement is done, followed by a period T_0 without field where the measurement of the disequilibrium is possible and effective. Then the same sequence of duration $T_{\rm tot} = T_{\rm St} + T_0$ is repeated up to the end of the conversion as shown in Figure 3.

Since we shut down the lock-in amplifier during the period $T_{\rm St}$, the signal needs some time to represent the real value of the enrichment when the period T_0 has begun. For this reason we choose our representative point near the end of this period. From this point the system experiences a period δT with zero field, then varying field during $T_{\rm St}$, and then $T_0 - \delta T$ with zero field. This is repeated during the experiment and gives the data points plotted as filled squares in Figure 3. After $T_{\rm tot}$ the signal is

$$\begin{aligned} S(t+T_{\rm tot}) &= S(t)\mathrm{e}^{-\gamma_0 \delta T}\mathrm{e}^{-\gamma_{\rm St} T_{\rm St}}\mathrm{e}^{-\gamma_0 (T_0 - \delta T)} \\ &= S(t)\mathrm{e}^{-(\gamma_{\rm St} T_{\rm St} + \gamma_0 T_0)} \\ &= S(t)\mathrm{e}^{-\gamma_{\rm exp} T_{\rm tot}}, \end{aligned} \tag{13}$$

where γ_0 is the spin conversion rate at zero field and $\gamma_{\rm St}$ is the conversion rate in the presence of the alternating triangular electric field scheme. Equation (13) is the definition of the rate that is extracted by fitting the curve given by the filled squares:

$$\gamma_{\rm exp} T_{\rm tot} = \gamma_{\rm St} T_{\rm St} + \gamma_0 T_0. \tag{14}$$

The uncertainty on the voltage applied between electrodes is about 1% using a multi-meter giving true RMS value. The voltage amplitude is simply $\sqrt{3} V_{\rm RMS}$ for an alternating triangular function.

Although the thickness of the spacers (0.080 cm) between electrodes is quite accurate, in the range of a few microns, the building and gluing of the cells leads to an inhomogeneity in the Stark field. Careful field calibration has been performed using the Stark spectroscopy technique within the sample cell [26]. This gives an average spacing of $d = 0.0878 \pm 0.0005$ cm with a dispersion of the electrode separation of $\pm$ 3.5%. This field inhomogeneity does not affect the measurement of the conversion rate substantially when an alternating field is used.

The electric field does not fill the whole volume: the volume $V_{\rm cell}$ is made with the volume located between the electrodes $V_{\rm St}$ and the volume of the glass tube up to the closing valve V_0 not submitted to the field (Fig. 2a). The diffusion time is negligible between these volumes $V_{\rm St}$ and V_0 and we have then to consider a weighted average over the volume for the conversion rate. Thus $\gamma_{\rm St}$ in (14) has to be replaced by $\gamma'_{\rm St}$ with

$$(V_0 + V_{\rm St})\gamma'_{\rm St} = \gamma_{\rm St} V_{\rm St} + \gamma_0 V_0. \tag{15}$$

Combining the average in time and in volume the measured rate is

$$\gamma_{\rm exp} = \eta\beta\gamma_{\rm St} + (1 - \eta\beta)\gamma_0 \tag{16}$$

with

$$\eta = \frac{V_{\rm St}}{V_0 + V_{\rm St}} \qquad \text{and} \qquad \beta = \frac{T_{\rm St}}{T_0 + T_{\rm St}} \cdot$$

Equation (16) clearly shows the symmetric role of the partitioning in volume and in time performed in our measurement of the conversion rate. By comparing to a calibrated volume we have been able to measure a sample cell volume of $V_{\rm cell} = 1.786 \pm 0.032$ cm^3. From the geometry of the spacers we know the effective volume submitted to the electric field to be $V_{\rm St} = 0.955 \pm 0.012$ cm^3 for $d = 0.0878$ cm; this gives $\eta = 0.535 \pm 0.011$. The uncertainty of η is an estimated error on the absolute accuracy of the volumes. The temporal sequence is synchronized by the computer and the precision on the intervals $T_{\rm St}$ and T_0 is a few milliseconds on durations of 3 to 10 seconds, so the uncertainty of β is negligible. The last correction that should be considered to the conversion rate to include is the wall contribution. It depends on the internal surface of the cell. We assume that the glass portion and the gold-coated electrodes have the same behavior [27] with a constant contribution $\gamma_{\rm wall}$ independent of the field strength. Consequently, equation (16) should be modified as:

$$\gamma_{\rm exp} = \gamma_{\rm wall} + \eta\beta\gamma_{\rm St} + (1 - \eta\beta)\gamma_0 \qquad (17)$$

in which $\gamma_{\rm St}$ and γ_0 are purely volumic contributions.

5 Results

In order to determine the wall contribution $\gamma_{\rm wall}$ to the conversion rate, we first measured the rate $\gamma_{\rm exp}$ for different pressures in the absence of electric field ($\beta = 0$). As has already been shown [14], the curve is a straight line from which $\gamma_{\rm wall}$ and $\gamma_0^P P$ can be deduced.

$$\gamma_{\rm exp} = \gamma_{\rm wall} + \gamma_0 = \gamma_{\rm wall} + \gamma_0^P P \qquad (18)$$

$$\gamma_{\rm exp}({\rm s}^{-1}) = 7.5(1.5) \times 10^{-4} + 11.67(0.52) \times 10^{-3}\, P \qquad (19)$$

where the pressure is given in torr (1 torr = 133 Pa). $\gamma_{\rm wall}$ is the intercept of the straight line with the γ axis at zero pressure.

Measurements were then performed for different pressures (up to 0.6 torr) and with different amplitudes of the triangular alternating field in the range 0 to 10 kV/cm. Pressures of 0.2–0.3 torr were preferred as the enrichment process is very efficient in this domain. These measurements complement those of reference [14] where only one electric field value of 1 070 V/cm for different pressures was applied in a Stark cell separated from the probe cell.

From each enrichment-conversion signal, a series of data points chosen as indicated in the previous section was fitted to an exponential curve using the least-squares fit method. From this measurement of $\gamma_{\rm exp}$, the value of $\gamma_{\rm St}$ was derived in accordance with equation (17), knowing the corresponding pressure P, and the η and β values. All the data are reported in Figure 4. We recorded some conversion signals for the same amplitude of the electric field and different values of β, checking that the derived values of $\gamma_{\rm St}$ are the same. The β value was chosen depending on the conversion rate expected; $T_{\rm St} = T_0 = 5$ s ($\beta = 0.5$) was often used for $F < 4\,000$ V/cm, while $T_{\rm St} = 3$ s, $T_0 = 7$ s ($\beta = 0.3$) was preferred for $F > 4\,000$ V/cm because the conversion with this field value is faster. The error bars represent the uncertainty in the exponential fitting procedure plus the uncertainty of the conversion rate without field.

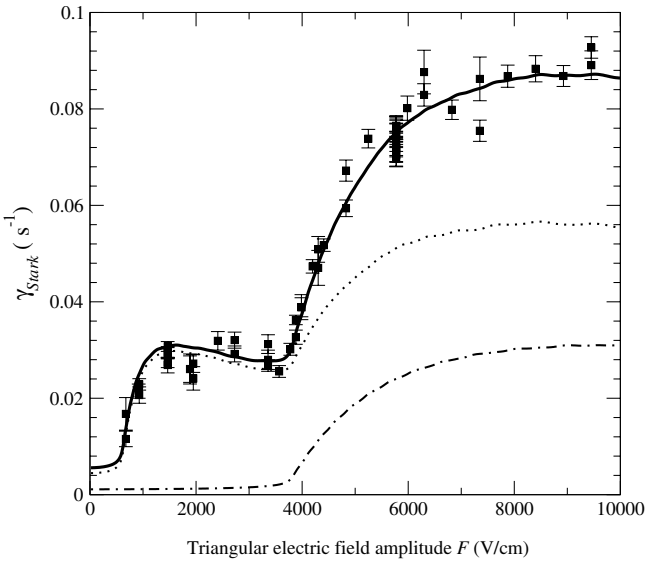

Fig. 4. Experimental data compared with the model with adjusted parameters. Squares with error bars are the experimental data points, the solid curve is the best fitted curve within the model, the dotted curve is the spin-spin contribution of the two pairs, and the dash-dotted curve is the spin-rotation contribution of the second pair only.

The general shape agrees with the lower part of Figure 1 which confirms the validity of the quantum relaxation model. For electric field values below 600 V/cm, the conversion rates remain low. Between 600 and 3 800 V/cm, crossings of the Stark components of the first pair lead to an increase of the conversion rate leading to a first plateau. Fields higher than 3 800 V/cm permit crossings involving the second pair. Conversion in this case is much faster and increases up to a second plateau. This gives, for the first time, experimental evidence of the role of the second pair $(J, K/J', K') = (21, 3/20, 1)$ in spin conversion. The positions for the sharp rises in the experimental results are well reproduced by the calculation. This confirms the quality of the spectroscopic data. The heights of the experimental plateaus are different from those calculated in the lower part of Figure 1. These heights depend mainly on the strength of the interaction parameters: the first plateau is the contribution of the crossings of the M-components of the first pair and depends on the spin-spin interaction only; the second plateau involves the second pair and depends on both spin-spin and spin-rotation interactions. The collisional relaxation rates have minor

Table 2. Comparison of previous results with this work.

Parameter	Previous measurement	Theory	This work
$\Gamma_{11,1/9,3}/P$ (10^8 $s^{-1}torr^{-1}$)	1.09 [(1)]		1.03
$\Gamma_{21,1/20,3}/P$ (10^8 $s^{-1}torr^{-1}$)	1.00 [(1)]		0.94
$\mathcal{T}_{22}$ (kHz)	69.6[(2)]	69.2 [(3)]	77
C_{22} (kHz)	≈ 2.1 [(4)]		1.52

[(1)]Reference [25], [(2)]reference [14], [(3)] calculated from average structure on vibrational ground state [18,20], [(4)] estimated by Gus'kov [17] from experimental value of spin conversion with zero field.

effects on these heights as a result of the integration technique but their values influence the conversion rate at zero field.

The next step is to fit all the experimental data taken at different pressures, assuming a possible variation of $\mathcal{T}_{22}$, C_{22} and $\Gamma_{\alpha\alpha'}$. The $\Gamma_{\alpha\alpha'}$ values of the two pairs are varied keeping constant the ratio $\Gamma_{20,21}/\Gamma_{9,11} = 0.91$, which reflects the expected J dependence of the relaxation rates [25]. Each experimental conversion rate was compared with the value calculated at the same pressure and for the same field strength. A least square fit method gives the best set of values for $\mathcal{T}_{22}$, C_{22} and $\Gamma_{\alpha\alpha'}$. Except for those at zero field, all the experimental rates with their respective uncertainties are drawn as filled squares in Figure 4. To illustrate the result of the fit, we draw the calculated curve for a pressure of 0.3 torr. As the pressure dependence is small (see Fig. 1 lower part), this curve efficiently supports the comparison with all experimental points. The dotted curve corresponds to the spin-spin contribution for the two pairs and the dash-dotted curve to the spin-rotation contribution of the second pair. The results of the fit are $\mathcal{T}_{22} = 77(2)$ kHz, $C_{22} = 1.52(5)$ kHz and the starting $\Gamma_{\alpha\alpha'}$ values have to be multiplied by 0.94(4) (Tab. 2). The value of the reduced χ-square is around 3, which expresses the dispersion of the data.

6 Discussion

The comparison of the experimental and calculated spin conversion rate in the framework of the quantum relaxation model is satisfactory and confirms the validity of the model. In particular the role of the second pair is demonstrated. Some discrepancies remain that are discussed below.

Our method allows us to determine quasi independently three parameters, spin-spin, spin-rotation and one relaxation rate, linked respectively to the values of the two plateaus and to the value of Γ_0^P at zero field. The spin-spin term $\mathcal{T}_{22} = 77 \pm 2$ kHz is 12% higher than the value obtained from our previous measurement [14] 69.6 ± 1 kHz which was very near to the theoretical value derived from the molecular structure 69.2 ± 0.2 kHz. No really convincing explanations are found for this discrepancy. The set-up and the method used are considerably different. In the previous experiment, the Stark cell was separated from the sample cell, giving more importance to the diffusion process. Only one field strength (1 070 V/cm) was studied, corresponding to the first rise in the curve drawn in the lower part of Figure 1. Our new cell is designed for fast conversion in high field and the time sequence is precise. In both set-ups, the results depend on the precise measurement of the volumes with and without Stark field. The discrepancy in the value of the spin-spin term leads to a variation of +24% on the conversion rates. Note that this behavior was observed previously at a lower level of accuracy in measurement with a sinusoidal alternating field [13] where the difference between theory and experiment observed in conversion rates was nearly zero for fields lower than 1 100 V/cm and suddenly jumped to +14% for field strengths greater than 1 100 V/cm.

The theoretical value itself is calculated with certain approximations. Firstly, within equations (3, 4), the rigorous calculation would be the average of the spin-spin interaction ($1/r^3$ and angular dependence) over the instantaneous structure of the vibrational ground state. Such calculations are difficult and tedious. Secondly these formulae are only first order calculations of the possible spin-spin interactions.

Our new results could be affected by systematic errors (for example errors of volume affecting the η value and decreasing or increasing globally all the values of conversion rates). In the fitting procedure, different attempts were made keeping the spin-spin term fixed to the theoretical value or the spin-rotation term to zero. In the first case, the fitted curve does not succeed in satisfactorily reproducing the first plateau, but the agreement is adequate for the second plateau with a spin-rotation strength of $C_{22} = 1.82(5)$ kHz. In the second case, no satisfactory fit was found, clearly demonstrating that a second interaction occurs in the spin conversion of the second pair. The spin-rotation interaction hypothesis agrees well with the selection rules valid for the two involved pairs. An interaction strength of $C_{22} = 1.5(4)$ kHz is deduced from our experiment. It represents the off-diagonal electronic part of the spin-rotation tensor. It is in the same order of magnitude as the diagonal components obtained by fitting hyperfine spectra (perpendicular component $C_\perp = 0.8 \pm 1.5$ kHz, parallel component $C_{zz} = 14.66 \pm 0.7$ kHz) [21].

7 Conclusion

Our experiment clearly confirmed the model of quantum relaxation proposed by Chapovsky. In particular it demonstrated directly the role of the two pairs of levels involved

in the process of conversion for $^{13}CH_3F$. The behavior of the first pair $(J', K'/J, K) = (11, 1/9, 3)$ in an electric field was already studied experimentally [12–14]. In our work, reaching higher field strength revealed for the first time the role of the second pair $(J', K'/J, K) = (21, 1/20, 3)$. For this pair, the selection rules are such that both spin-spin and spin-rotation interactions are involved. Their respective strengths were measured. Although some discrepancies remain in the comparison between experiment and theory, the role of spin-rotation interaction in spin conversion is demonstrated. In addition, it provides the first measurement of the transverse anisotropy $C_{22} = \Delta C_\perp = (C_{xx} - C_{yy})/2 = \Delta E_\perp = 1.52(5)$ kHz where only the electronic part of the spin-rotation interaction is involved. This value has an order of magnitude comparable to that of the diagonal components of the tensor. Extension of the work reported here to $^{12}CH_3F$ is planned, where four pairs of levels are involved with different $\Delta J/\Delta K$ values than in $^{13}CH_3F$ [10,17]. The role of the relaxation rate of the coherence between ortho and para states $\Gamma_{\alpha\alpha'}$ was removed on purpose by our experimental scheme, but it remains an important parameter of the spin conversion process. Its measurement could be a new challenge, in particular the possible dependence on M, M' sub-levels.

The authors are very thankful to E. Delbos for his help in the design of the cells. This work is part of the scientific program of the Centre d'Études et de Recherches Lasers et Applications (CERLA) which is supported by the Ministère de la Recherche, the Région Nord-Pas de Calais and the Fonds Européen de Développement Économique des Régions.

References

1. K.F. Bonhoeffer, P. Harteck, Naturwiss. **17**, 182 (1929)
2. L.N. Krasnoperov, V.N. Panfilov, V.P. Strunin, P.L. Chapovsky, JETP Lett. **39**, 143 (1984)
3. P.L. Chapovsky, J. Cosléou, F. Herlemont, M. Khelkhal, J. Legrand, Chem. Phys. Lett. **322**, 424 (2000)
4. J. Kern, H. Schwahn, B.Schramm, Chem. Phys. Lett. **154**, 292 (1989); G. Peters, B. Schramm, Chem. Phys. Lett. **302**, 181 (1999)
5. V.K. Konyukhov, A.M. Prokhorov, V.I. Tikhonov, V.N. Faĭzulaev, JETP Lett. **43**, 65 (1986)
6. D. Uy, M. Cordonnier, T. Oka, Phys. Rev. Lett. **78**, 3844 (1997)
7. R.A. Bernheim, C. He, J. Chem. Phys. **92**, 5959 (1990)
8. P.L. Chapovsky, L.J.F. Hermans, Annu. Rev. Phys. Chem. **50**, 315 (1999)
9. R.F. Curl Jr, J.V.V. Kasper, K.S. Pitzer, J. Chem. Phys. **46**, 3220 (1967)
10. P.L. Chapovsky, Phys. Rev. A **43**, 3624 (1991)
11. P.L. Chapovsky, Physica A **233**, 441 (1996)
12. B. Nagels, N. Calas, D.A. Roozemond, L.F.F. Hermans, P.L. Chapovsky, Phys. Rev. Lett. **77**, 4732 (1996)
13. J. Cosléou, F. Herlemont, M. Khelkhal, J. Legrand, P.L. Chapovsky, Eur. Phys. J. D **10**, 99 (2000)
14. P.L. Chapovsky, J. Cosléou, F. Herlemont, M. Khelkhal, J. Legrand, Eur. Phys. J. D **12**, 297 (2000)
15. W.H. Flygare, J. Chem. Phys. **41**, 793 (1964)
16. E. Ilisca, K. Bahloul, Phys. Rev. A **57**, 4296 (1998)
17. K.I. Gus'kov, J. Phys. B: At. Mol. Opt. Phys. **32**, 2963 (1999)
18. J. Demaison, J. Breidung, W. Thiel, D. Papousek, Struct. Chem. **10**, 2 (1999)
19. D. Papousek, J. Demaison, G. Wlodarczak, P. Pracna, S. Klee, M. Winnewisser, J. Mol. Spec. **164**, 351 (1994)
20. T. Egawa, S. Yamamoto, M. Nakata, K. Kuchitsu, J. Mol. Structure **156**, 213 (1987)
21. S.C. Wofsy, J.S. Muenter, W. Klemperer, J. Chem. Phys. **55**, 2014 (1971)
22. P. Bréchignac J. Chem. Phys. **76** , 3389 (1982)
23. B. Nagels, M. Schuurman, P.L. Chapovsky, L.J.F. Hermans, Chem. Phys. Lett. **242**, 48 (1995)
24. K. Bahloul, M. Irac-Astaud, E. Ilisca, P.L. Chapovsky, J. Phys. B: At. Mol. Opt. Phys. **31**, 73 (1998)
25. N.J. Trappeniers, E.W.A. Elenbaas-Bunschotten, Chem. Phys. Lett. **64**, 205 (1979)
26. S.M. Freund, G. Duxbury, M. Römheld, J.T. Tiedje, T. Oka, J. Mol. Spec. **52**, 38 (1974)
27. B. Nagels, Ph.D. thesis, Leiden University, The Netherlands, 1998